Vol 15 No 9, September 2006
1009-1963/2006/15(09)/2158-07
Chinese Physics
© 2006 Chin. Phys. Soc.
and IOP Publishing Ltd

Effects of Nb_2O_5 on thermal stability and optical properties of Er^{3+}-doped tellurite glasses*

Zhao Chun(赵 纯)[a)b)†], Zhang Qin-Yuan(张勤远)[a)‡],
Pan Yue-Xiao(潘跃晓)[a)], and Jiang Zhong-Hong(姜中宏)[a)]

[a)] *Key Laboratory of Special Functional Materials and Advanced Manufacturing Technology (Ministry of Education) and Institute of Optical Communications, South China University of Technology, Guangzhou* 510641, *China*

[b)] *College of Applied Physics, South China University of Technology, Guangzhou* 510641, *China*

(Received 28 September 2005; revised manuscript received 9 May 2006)

Er^{3+}-doped tellurite glasses with molar compositions of $x$$Nb_2O_5$ – (14.7 – x)Na_2O–10ZnO–5K_2O–10GeO_2–60TeO_2–0.3Er_2O_3 ($x = 0, 3, 5, 7$ and 9) have been investigated for developing 1.5 μm fibre and planar amplifiers. The effects of Nb_2O_5 on the thermal stability and optical properties of Er^{3+}-doped tellurite glasses have been discussed. It is noted that the incorporation of Nb_2O_5 ($x = 5$) increases the thermal stability of tellurite glasses significantly. Er^{3+}-doped niobium tellurite glasses exhibit a large stimulated emission cross-section ($7.2 \times 10^{-21} - 10.7 \times 10^{-21}$ cm^2) and the gain bandwidth, FWHM$\times\sigma_e^{peak}$ ($274 \times 10^{-28} - 480 \times 10^{-28}$ cm^3), which are significantly higher than that of silicate and phosphate glasses. In addition, the intensity of upconversion luminescence of the Er^{3+}-doped niobium tellurite glasses decreases rapidly with increasing Nb_2O_5 content. As a result, Er^{3+}-doped niobium tellurite glasses might be a potential candidate for developing laser or optical amplifier devices.

Keywords: glasses, thermal analysis, optical materials, optical properties
PACC: 7855, 4255R, 7840

1. Introduction

Glasses based on tellurium oxide doped with Er^{3+} ions can provide a broadband amplification around 1530 nm ($^4I_{13/2} \rightarrow {}^4I_{15/2}$ transition), and tellurite glasses, possess a number of advantages over the conventional oxides glasses, including a wide transmission region ($0.35 - 5$ μm), good corrosion resistance, and low phonon energy (~ 800 cm^{-1}).[1–4] Over the past several years, tellurite glasses have attracted a great deal of attention not only in fundamental research but also in optical devices fabrication for their good electrical, optical and magnetic properties.[1,5,6]

Although tremendous progress has been made, some difficulties such as a low thermal stability and a strong upconversion luminescence, etc., have so far been hindering the Er^{3+}-doped tellurite glasses devices from their full commercialization.

The main objective of this work is to carry out a detailed study on the spectral properties and thermal stability of Er^{3+}-doped niobium tellurite glasses $x$$Nb_2O_5$ – (14.7 – x)Na_2O–10ZnO–5K_2O–10GeO_2–60TeO_2–0.3Er_2O_3 ($x = 0, 3, 5, 7$ and 9), to examine their suitability as potential optical glasses for fibre amplifiers.

2. Experiment

In this work, glasses with molar compositions of $x$$Nb_2O_5$ – (14.7 – x)Na_2O–10ZnO–5K_2O–10GeO_2–60TeO_2–0.3Er_2O_3 ($x = 0, 3, 5, 7, 9$, referred to as N_0, N_1, N_2, N_3 and N_4 respectively) were prepared using analytic purity powders of Na_2CO_3, K_2CO_3, ZnO, Nb_2O_5, GeO_2, and TeO_2. Er^{3+} ion was introduced from high purity powders of Er_2O_3. Batches of 20 g were well mixed and melted in a covered platinum crucible at 850 °C for 15 min in a SiC-resistance electric furnace. The liquids were cast on a preheated stainless-steel mould and moved into a muffle furnace for 2 h at a temperature above the glass tran-

*Project supported by the National Natural Science Foundation of China (Grant No 50472053), New Century Excellent Talent Program in University of China (Grant Nos 04-0821 and 04-0823), Guangzhou Science and Technology Program of China (Grant No 2004Z2-D0131), and Youth Nature Science Foundation of South China University of Technology (Grant No 123-E5040900).
†E-mail: zhaochun@scut.edu.cn
‡Corresponding author. E-mail: qyzhang@scut.edu.cn

sition. The annealed samples were cut into specimens of 20 mm× 10 mm×2 mm and optical-polished.

Thermal analyses of glasses were examined by a Netzsch STA 449C Jupiter differential scanning calorimeter (DSC) at a heating rate of 10 $K\cdot min^{-1}$ from room temperature to 700 °C. Raman scattering spectra were obtained using a microscope spectrophotometer (model RM 2000, Renishaw, England) with 514.5 nm laser as the excitation source and the working power is 20 mW. The Raman spectra were recorded in the wavenumber range of 250–1000 cm^{-1}. In order to compare the stretching vibrations of the samples with different compositions as accurate as possible, the laser power level and scan frequency were fixed under the same condition.

The absorption spectra were recorded by a Perkin Elmer Lambda-900 UV/VIS/NIR spectrophotometer ranging from 350 to 1700 nm with a resolution of 1 nm. Fluorescence spectra and upconversion luminescence spectra were measured on the TRIAX320 type spectrometer (Jobin–Yvon Co., France) with 977 nm LD as an excitation source. In order to compare the fluorescence intensities in different samples, the position and power (600 mW) of the pumping beam and the width (0.5 mm) of the slit to collect the luminescence signal were kept constant. The fluorescence lifetimes were measured by exciting the samples with the 977 nm LD and detected by a photon-counting R5108 photomultiplier tube. All the measurements were performed at room temperature.

3. Results and discussion

The various properties of the glasses with different compositions are summarized in Table 1. The densities and refractive indices of these samples increase with increasing Nb_2O_5 content added in the tellurite glasses.

Table 1. Density, refractive indices and thermal properties of $x$$Nb_2O_5$ $-(14.7-x)$ Na_2O–10ZnO–5K_2O–10GeO_2– 60TeO_2 ($x = 3, 5, 7, 9$).

sample	density/g$\cdot$ cm^{-3}	refractive indices	T_g/℃	T_x/℃	$T_x - T_g$/℃
N_0	4.70	1.94	262.7	-	-
N_1	4.75	1.98	300.6	-	-
N_2	4.78	2.00	317.1	-	-
N_3	4.82	2.03	335.4	422.9	87.5
N_4	4.86	2.05	352.8	460.0	107.2

The DSC curves of N_0, N_1, N_2, N_3, and N_4 are illustrated in Fig.1. Glass transition temperature (T_g), crystallization onset temperature (T_x), and ΔT ($\Delta T = T_x - T_g$) are shown in Table 1. T_g increases significantly with substitution of Nb_2O_5 for Na_2O, while no obvious crystallization peak is detected in N_0, N_1, N_2 samples. T_g increases with Nb_2O_5 content monotonically while $T_x - T_g$ increases initially and then decreases with increasing content of Nb_2O_5. When the content of Nb_2O_5 is 5 mol%, the glass presents the best thermal stability. The evolution of T_g for Na/Nb substitution can be easily explained since the glass transition involves the breaking of the chemical bonds. The bond energy of Nb–O is larger than that of Na–O because the charge densities of Nb^{5+} is larger than that of Na^+, so the substitution of Nb_2O_5 for Na_2O leads to the increase of the T_g values. In addition, the obvious increase of T_g also indicates a restructuring of the network. The evolution of ΔT may be explained as follows: the electronegativity of Nb ($x_{Nb} = 1.6$) is a large, which results in a large attraction between Nb^{5+} ion and the neighbouring glass-forming units. So the thermal stability increases when its content is lower than 5 mol%. When the concentration of Nb_2O_5 is over 5 mol% in the glasses, more nonbridging oxygens are produced, which results in destroying the network and decreasing the thermal stability. This result is not consistent with that in Ref.[7]. Effect of Nb_2O_5 on thermal properties may be connected with the host of glasses.

The thermal stability factor ΔT is frequently used as a rough estimate of the glass stability. To achieve a large working range of temperature during sample fibre drawing, it is desirable for a glass host to have ΔT as large as possible.[5] As shown in Fig.1, no obvious crystallization peak is detected at a heating rate of 10 $K\cdot min^{-1}$ for the samples of N_0, N_1, and N_2, indicating that these glasses are much preferable for performing fabrication and crystal-free fibre drawing.[2,8]

The Raman spectra of N_4 and N_0 shown in Fig.2

are composed of three spectral regions: (i) a low-frequency region (< 300 cm^{-1}), which is attributed to the collective modes of local structures and heavy metal vibrational modes;[9] (ii) an intermediate region (300–650 cm^{-1}), which is attributed to the deformation of vibrational modes of a glass network structure with bridged oxygen,[10–12] and (iii) a high-frequency region (> 650 cm^{-1}), which is attributed to the stretching vibrational modes of the glass network former.[11,12] In the intermediate region, the bands of N_4 around 462 cm^{-1} originate from the stretching vibrations in Ge–O–Ge and Te–O–Te. In the high-frequency region, the bands around 688 cm^{-1} originate from TeO_4 and those at 764 cm^{-1} originate from TeO_{3+1}, TeO_3 and GeO_6. The maximum phonon energy of N_0 is 757 cm^{-1} which is slightly lower than that of N_4, and the intensity of these peaks are lower than N_4 demonstrating that Nb_2O_5 increases the phonon energy and the phonon energy density in these tellurite glasses.

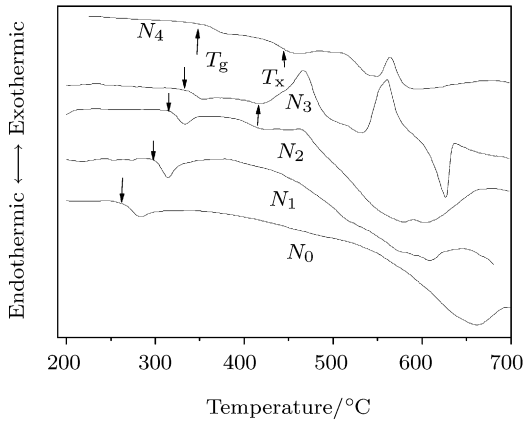


Fig.1. DSC curves of $x$$Nb_2O_5$ − (14.7 − x)Na_2O–10ZnO–5K_2O–10GeO_2–60TeO_2 (x = 0, 3, 5, 7, 9) glasses.

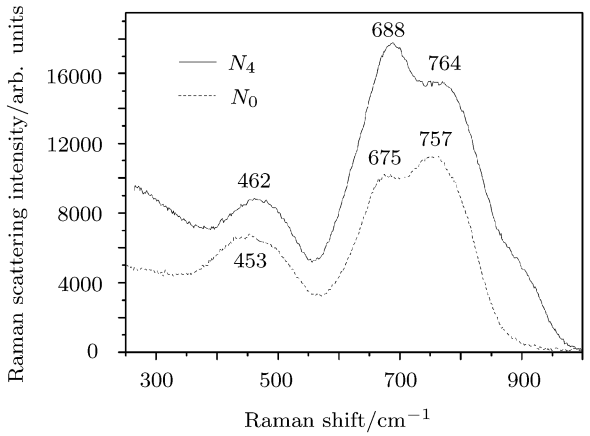


Fig.2. Raman spectra of $x$$Nb_2O_5$–(14.7 − x)Na_2O–10ZnO–5K_2O–10GeO_2–60TeO_2 ($x = 0, 9$) glasses.

Figure 3 shows the room temperature optical absorption spectra for these tellurite glasses in the 350–1700 nm spectral range. The inhomogeneously broadened bands are assigned to the transitions from the ground state $^4I_{15/2}$ to the excited states of Er^{3+} ions.

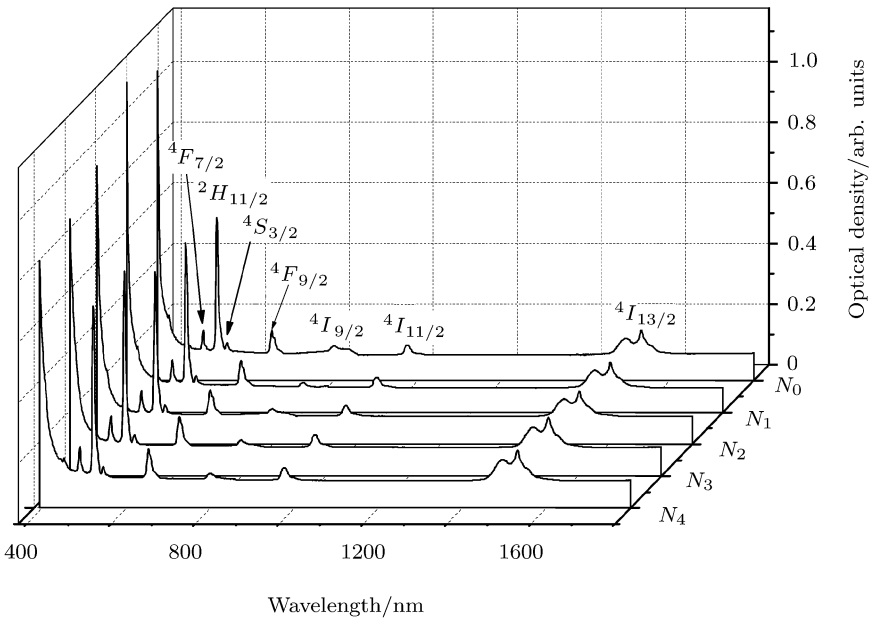


Fig.3. Absorption spectra of Er^{3+}-doped $x$$Nb_2O_5$ − (14.7 − x)Na_2O–10ZnO–5K_2O–10GeO_2–60TeO_2 ($x = 0, 3, 5, 7, 9$) glasses.

Judd–Ofelt intensity parameters Ω_t $(t = 2, 4, 6)$ have been calculated from the absorption spectra in Fig.3 by using the Judd–Ofelt theory. Figure 4 illustrates the compositional dependence of Ω_t $(t = 2, 4, 6)$ parameters of sample glasses. Apparently, Ω_2, Ω_4 and Ω_6 increase with increasing Nb_2O_5 content.

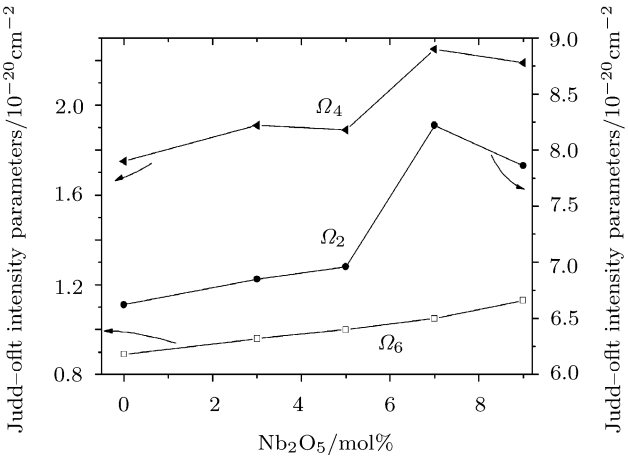


Fig.4. Judd–Ofelt intensity parameters of $x$$Nb_2O_5$–$(14.7-x)$$Na_2O$–10ZnO–5$K_2O$–10$GeO_2$–60$TeO_2$–0.3$Er_2O_3$ $(x = 0, 3, 5, 7, 9)$ glasses.

As is known, Ω_2 is related with the symmetry of the glass host, while Ω_6 is inversely proportional to the covalency of Er–O bond. The larger the Ω_2, the more asymmetric the glass host. Ω_2 in the present glasses changes from 6.62×10^{-20} cm^{-2} to 7.86×10^{-20} cm^{-2} which is larger than that in germanate (= 5.81×10^{-20} cm^{-2}), silicate (= 4.23×10^{-20} cm^{-2}), and aluminate (= 5.6×10^{-20} cm^{-2}) glasses.[13] Ω_6 changes from 0.89×10^{-20} cm^{-2} to 1.13×10^{-20} cm^{-2}. These values are comparable to the Ω_6 of fluoride (1.11×10^{-20} cm^{-2}) glass[14] but larger than that of silicate (0.61×10^{-20} cm^{-2}), aluminate (0.61×10^{-20} cm^{-2}) and germinate (0.28×10^{-20} cm^{-2}) glasses.[13] These differences indicate that the covalency of Er–O bond in the present glasses is lower than that in germanate, silicate, aluminate and phosphate glasses.[4] According to the electronegativity theory, the smaller the difference of electronegativity between cation and anion ions, the stronger the covalency of the band. Since the values of electronegativity, for Na, Nb and O elements, are 0.9, 1.6 and 3.5, respectively, the covalency of Nb–O bond is stronger than Na–O. It is expected that effects of Nb–O on the local ligand environments around Er^{3+} increase with Nb_2O_5 content. Consequently, the covalency of the Er–O bond decreases, and the value of Ω_6 increases accordingly.

Lifetimes of $^4I_{13/2}$ levels of Er^{3+} in $x$$Nb_2O_5$–$(14.7-x)$$Na_2O$–10ZnO–5$K_2O$–10$GeO_2$–60$TeO_2$–0.3$Er_2O_3$ $(x = 0, 3, 5, 7, 9)$ are also investigated and the compositional dependence of measured fluorescence lifetimes are illustrated below in Fig.7, from which we see that the fluorescence lifetime of the $^4I_{13/2}$level decreases with an increase of Nb_2O_5 content. The interaction between Nb^{5+} and O^{2-} ions is contributed to the nonradiative decay of the $^4I_{13/2}$ level.

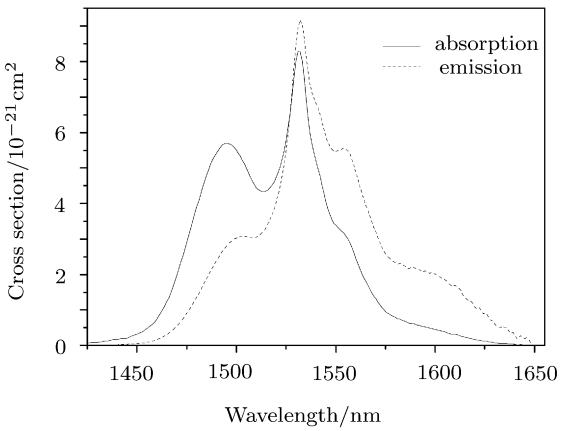


Fig.5. The calculated absorption and emission cross-sections of Er^{3+}-doped 5Nb_2O_5–9.7Na_2O–10ZnO–5K_2O–10GeO_2–60TeO_2 glass in the wavelength range of 1420–1630 nm under the 977 nm excitation at room temperature.

The absorption cross section (σ_{abs}) is determined from the absorption spectra and the stimulated emission cross section (σ_e) is evaluated by the McCumber theory:[15]

$$\sigma_e(\lambda) = \sigma_{abs}(\lambda)\exp\Big[\frac{1}{kT}(\varepsilon - h\nu)\Big],$$

where ν is the photon frequency, k is the Boltzmann constant, and ε is the net free energy required to excite one Er^{3+} from the ground state $^4I_{15/2}$ to the excited state $^4I_{13/2}$ at temperature T, and the value is calculated using the procedure provided by Ref.[16]. Table 2 shows the absorption cross-section values and emission cross-section values of the transition $^4I_{13/2}\rightarrow{}^4I_{15/2}$ of Er^{3+} in the glasses. The calculated absorption and emission cross-sections of N_2 glass in the wavelength range of 1420–1630 nm under the 977 nm excitation are illustrated in Fig.5. Since the stimulated emission cross section is proportional to the host glass refractive index, $\sigma_e \sim (n^2+2)^2/n$,[2] it is apparent that Er^{3+} ions in the glasses with more Nb_2O_5 are capable of providing large stimulated emission cross section at 1.53 μm.

Table 2. Emission parameters of Er^{3+} at 1532 nm emission in various glasses systems.

sample	FWHM/nm	$\sigma_e^{peak}/10^{-21}$ cm^2	$\sigma_{abs}^{peak}/10^{-21}$ cm^2	FWHM$\times\sigma_e^{peak}$ $/\times10^{-28}$ cm^3	τ_f/ms	$\sigma_e^{peak}\times\tau_f$ $/10^{-21}$ cm$^2\cdot$ms
N_0	38	7.2	6.6	274	3.6	25.9
N_1	39	7.6	6.9	296	3.3	25.4
N_2	42	8.1	7.3	340	3.0	23.7
N_3	43	9.1	8.2	392	2.9	27.2
N_4	45	10.7	9.6	482	2.7	29.3
tellurite[17]	60	6.6	-	396	4	26.4
silicate[18]	45	5.5	-	247	10	55
phosphate[19]	37	6.4	-	237	8	51.2
fluorophosphates[20]	53	6.0		318	8	48

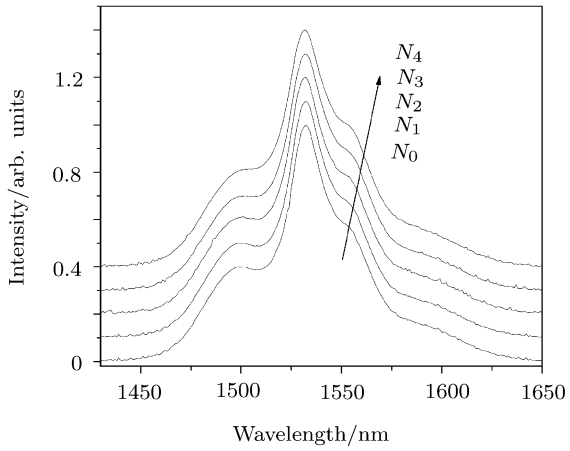


Fig.6. Normalized fluorescence spectra of xNb$_2$O$_5$ – (14.7 – x) Na$_2$O–10ZnO–5K$_2$O–10GeO$_2$–60TeO$_2$–0.3Er$_2$O$_3$ (x = 0, 3, 5, 7, 9) glasses excited by a 977 nm LD (Y-shift).

Figure 6 illustrates the normalized fluorescence spectra in the wavelength range 1440–1650 nm under 977 nm excitation. The broad 1.53μm emission is assigned to the $^4I_{13/2} \rightarrow ^4I_{15/2}$ transition. As an important parameter for optical amplifiers to realize broadband and the gain amplification, full width of half maximum (FWHM) and σ_e^{peak}can be used to evaluate the gain properties of the optical amplifiers. The gain bandwidth of an amplifier is determined mainly by the width of emission spectra. The values of FWHM $\times\sigma_e^{peak}$ and $\tau_f \times \sigma_e^{peak}$ are important parameters for erbium-doped fibre amplifier (EDFA). The larger the value of FWHM$\times\sigma_e^{peak}$, the wider the gain bandwidth. The larger the $\tau_f \times \sigma_e^{peak}$, the higher the gain character. FWHM, τ_f, FWHM$\times\sigma_e^{peak}$ and $\tau_f\times\sigma_e^{peak}$ are also compared in Table 2 and illustrated in Figs 7(a) and 7(b). The values of FWHM, σ_e^{peak}, FWHM$\times\sigma_e^{peak}$and $\tau_f \times \sigma_e^{peak}$ in tellurite increase with Nb_2O_5 content.

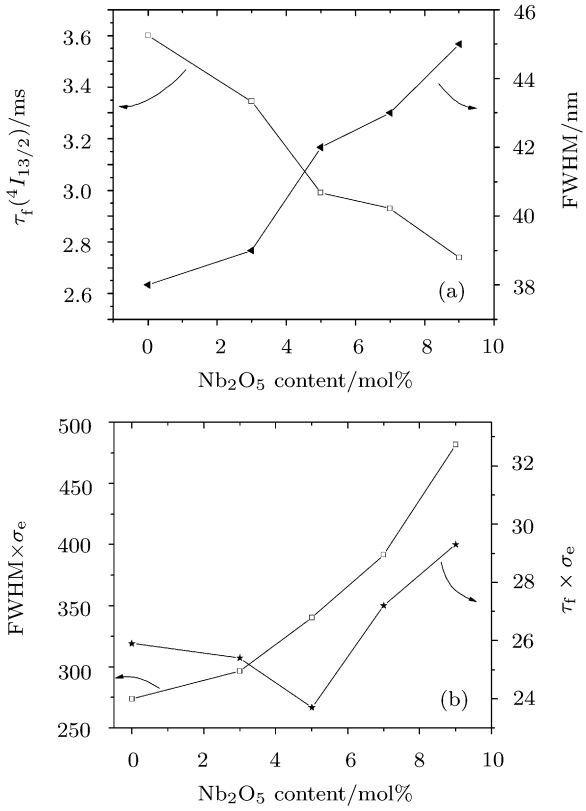


Fig.7. Compositional dependence of measured lifetime of $^4I_{13/2}$ level of Er^{3+} (τ_f) and FWHM. (b) Compositional dependence of FWHM$\times\sigma_e$ and $\tau_f \times \sigma_e$ in xNb$_2$O$_5$ – (14.7 – x) Na$_2$O–10ZnO–5K$_2$O– 10GeO$_2$–60TeO$_2$–0.3Er$_2$O$_3$ glasses (x = 0, 3, 5, 7, 9).

Figure 7(a) shows the compositional dependence of FWHM and τ_f, and 7(b) illustrates the compositional dependence of FWHM$\times\sigma_e$ and $\tau_f \times \sigma_e$ in xNb$_2$O$_5$ – (14.7 – x) Na$_2$O–10ZnO–5K$_2$O–10GeO$_2$–60TeO$_2$–0.3Er$_2$O$_3$ glasses. In Fig.7(a), the broadest

FWHM value of these glasses is about 49 nm, which is larger than that of phosphate glasses,[19] but is smaller than that of tellurite based glasses ($\approx$ 60 nm).[17]

The maximum values of σ_e^{peak}, FWHM$\times\sigma_e^{peak}$ are 10.7×10^{-21} cm^2, 482×10^{-28} cm^3 respectively. These values are much larger than that of silicate, phosphate glasses. The maximum values of $\tau_f \times \sigma_e^{peak}$ is 29.3×10^{-21} cm$^2\cdot$ ms that is larger than the value reported for tellurite glasses,[17] but is smaller than that of silicate, phosphate and fluorophosphates. FWHM and the lifetimes of $^4I_{13/2}$ in our glasses are expected to increase in the following work. Increasing Nb_2O_5 content is helpful to promote the amplification performance.

The spectra of frequency upconversion of Er^{3+}-doped glass samples in the visible wavelength range of 500–750 nm under 977 nm LD excitation at room temperature are shown in Fig.8.

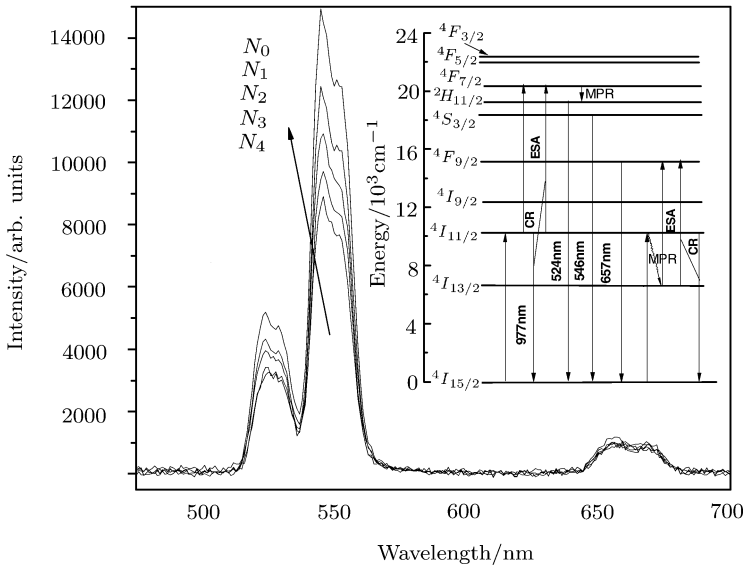


Fig.8. Visible upconversion luminescence spectrum of Er^{3+}-doped $xNb_2O_5 - (14.7 - x)$ Na_2O–10ZnO–$5K_2O$–$10GeO_2$–$60TeO_2$ ($x = 0, 3, 5, 7, 9$) glasses. The schematic energy level diagram of possible upconversion mechanisms of these glasses with 977 nm excitation and the possible upconversion emission mechanism is indicated (upon 977nm excitation at room temperature).

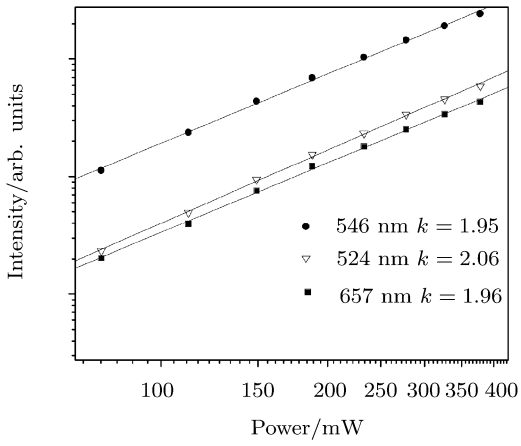


Fig.9. The dependences of the upconversion green and red emission intensities on pump laser power under excitation of 977 nm LD.

The spectra exhibit three distinct bands centred at 524, 546, 657 nm, which are assigned to the $^2H_{11/2} \rightarrow^4 I_{15/2}$, $^4S_{3/2} \rightarrow^4 I_{15/2}$, and $^4F_{9/2} \rightarrow^4 I_{15/2}$ transitions of Er^{3+}, respectively. In Fig.9, the green and red upconversion emission intensities versus pump power in log–log representation yield straight lines with different slopes (slope 1.96, 2.06, 1.95 for 524, 546 and 657 nm, respectively). The figure indicates that both 524 and 657 nm emissions are two-photon-process while 546 nm emissions might be mainly a two-photon-process with a less three-photon absorption.

The obvious decrease of the green upconversion emission with increasing content of Nb_2O_5 is depicted in Fig.8. The green luminescence intensity in the N_1,

N_2, N_3 and N_4 glasses decreases to 94%, 90 %, 70% and 61% of that in N_0 glass, respectively. But the red intensity is not affected apparently by the concentration of Nb_2O_5. The green upconversion emission intensity is mainly determined by the maximum phonon energies and the densities of maximum phonon energies density[21] of glasses while the red upconversion emission intensity is mainly determined by ESA process.[22,23] Our investigation indicates that increasing Nb_2O_5 content could improve the phonon energy and the density of maximum phonon energies of host glass, and thus promote the rate of multi-phonon relaxation and decrease the upconversion emissions.

4. Conclusion

We have systematically studied the effects of Nb_2O_5 on the thermal stability and optical properties of Er^{3+} ion in the tellurite glasses. In conclusion, adding Nb_2O_5 with appropriate content in tellurite glass is helpful to increase the maximum phonon energy and the maximum density of phonon energies, and improve thermal stability, stimulated emission cross section and FWHM of it. In addition, the upconversion green emissions are weaker and the fluorescence lifetimes of Er^{3+}: $^4I_{13/2}$ in Nb_2O_5-doped tellurite glasses are shorter than those in the tellurite glasses free of Nb_2O_5. In our study, the maximum stimulated emission cross-section, the largest values of FWHM$\times\sigma_e^{peak}$ and $\tau_f \times \sigma_e^{peak}$ of these series of glasses are 10.7×10^{-21} cm^2, 482×10^{-28} cm^3 and 29.3×10^{-21} cm$^2\cdot$ms, respectively. Therefore, they are suitable for the application in developing waveguide and optical amplifier devices.

References

[1] Dai S X, Wu J L, Zhang J J, Wang G N and Jiang Z H 2005 *Spectrochim. Acta Part* A **62** 431
[2] Wang J S, Vogel E M and Snitzer E 1994 *Opt. Mater.* **3** 187
[3] Petit L, Cardinal T, Videau J J, Durand E, Canioni L, Martines M, Guyot Y and Boulon G 2006 *Opt. Mater.* **28** 172
[4] Yamauchi H, Murugan G S and Ohishi Y 2005 *J. Appl. Phys.* **97** 043505
[5] Murugan G S and Ohishi Y 2004 *J. Non-Cryst. Solids* **341** 86
[6] Tikhomirov V K, Seddon A B, Furniss D and Ferrari M 2003 *J. Non-Cryst. Solids* **326**—**327** 296
[7] Chen D D, Liu Y H, Zhang Q Y, Deng Z D and Jiang Z H 2005 *Mater Chem. Phys.* **90** 78
[8] Kim S H and Yoko T 1995 *J. Am. Ceram. Soc.* 78 (4) 1061
[9] Pan Z, Henderson D O and Morgan S H 1994 *J. Non-Cryst. Solids* **171** 134
[10] Verweij H and Buster J 1979 *J. Non-Cryst. Solids* **34** 81
[11] Sekiya T, Mochida N and Ohtsuka A 1992 *J. Non-Cryst. Solids* **144** 128
[12] Burger H, Kneipp K and Hobert H 1992 *J. Non-Cryst. Solids* **151** 134
[13] Zou X L and Izumitani T 1993 *J. Non-Cryst. Solids* **162** 68
[14] Tanabe S 1999 *J. Non-Cryst. Solids* **259** 1
[15] McCumber D E 1964 *Phys. Rev.* A **134** 299
[16] Miniscalco W J and Quimby R S 1991 *Opt. Lett.* **16** 158
[17] Mori A, Ohishi Y, Yamada M, Ono H, Nishida Y, Oikawa K and Sudo S 1997 *Optical Fiber Communications'97*, PD1-l
[18] Shen S, Naftaly M and Jha A 1999 *Proc. SPIE.* **3849** 103
[19] Jiang S, Luo T, Hwang B C, Smekatala F, Seneschal K, Lucas J and Peyghambarian N 2000 *J. Non-Cryst. Solids.* **263** & **264** 364
[20] Zhang L Y and Hu L L 2003 *Chin. Phys. Lett.* **20** 1836
[21] Yang Z M and Jiang Z H 2004 *Chin. Sci. Bulletin* **49**(24) 2572
[22] Balda R, Oleaga A, Fernandez J and Fdez-Navarro J M 2003 *Opt. Mater.* **24** 83
[23] Li T, Zhang Q Y, Zhao C, Feng Z M , Shi D M, Deng Z D and Jiang Z H 2005 *Chin. Phys.* **14** 1250